Characterization of the Solution Structure of Human Serum Albumin Loaded with a Metal Porphyrin and Fatty Acids

Matthias J. N. Junk, Hans W. Spiess, and Dariush Hinderberger*
Max Planck Institute for Polymer Research, Mainz, Germany

ABSTRACT The structure of human serum albumin loaded with a metal porphyrin and fatty acids in solution is characterized by orientation-selective double electron-electron resonance (DEER) spectroscopy. Human serum albumin, spin-labeled fatty acids, and Cu(II) protoporphyrin IX—a hemin analog—form a fully self-assembled system that allows obtaining distances and mutual orientations between the paramagnetic guest molecules. We report a simplified analysis for the orientation-selective DEER data which can be applied when the orientation selection of one spin in the spin pair dominates the orientation selection of the other spin. The dipolar spectra reveal a dominant distance of 3.85 nm and a dominant orientation of the spin-spin vectors between Cu(II) protoporphyrin IX and 16-doxyl stearic acid, the electron paramagnetic resonance reporter group of the latter being located near the entry points to the fatty acid binding sites. This observation is in contrast to crystallographic data that suggest an asymmetric distribution of the entry points in the protein and hence the occurrence of various distances. In conjunction with the findings of a recent DEER study, the obtained data are indicative of a symmetric distribution of the binding site entries on the protein's surface. The overall anisotropic shape of the protein is reflected by one spin-spin vector orientation dominating the DEER data.

INTRODUCTION

Human serum albumin (HSA) is the most abundant protein in human blood plasma. It serves as a versatile transporter for numerous endogenous compounds and drug molecules (1,2). Its capability to bind and transport fatty acids (FA) is of particular physiological significance (3,4). Seven distinct binding sites for long chain FA were identified by crystallography, most of which comprise ionic anchoring units (positively charged amino-acid residues) and long, hydrophobic pockets (5,6). Counterintuitively, the FAs were found to be distributed asymmetrically in the protein crystal, although the protein itself exhibits a highly symmetric primary and secondary structure (5,7,8).

However, a crystallographic structure does not account for the dynamic conformational flexibility of a protein, which often constitutes a key parameter for its biological function (9,10). In particular, the surface-exposed parts of HSA show a high degree of flexibility and enable the protein to bind a large number of small molecules (11,12).

Triggered by these observations, we used an electron paramagnetic resonance (EPR) spectroscopic approach to determine the functional structure of HSA in solution. Replacing the fatty acids by their spin-labeled analogs, a self-assembled system is obtained, which allows the structural characterization of the protein from the point of view of the transported molecules (13,14).

The structural information is obtained by an EPR technique called double electron-electron resonance (DEER) spectroscopy (15–17), which utilizes the dipolar couplings between electron spins to allow distance measurements in the range of 1.5–8 nm (18). This intrinsically local technique has been increasingly used for the structural characterization of synthetic (19,20) and biological (21,22) macromolecular systems which lack long-range order (e.g., membrane proteins). It can, in principle, be used in two ways—either analyzing the time-domain data or the dipolar spectra after Fourier transformation (23).

By varying the position of the spin label in the hydrocarbon chain of the fatty acids, both the ionic anchor points of the binding sites in the protein's interior as well as the entry points into the fatty acid channels could be probed (13). The paramagnetic moiety of 5-DSA is located in the vicinity of the carboxylic acid group of the fatty acid which interacts with positively charged amino-acid residues in the binding channel, and is representative of these anchor points. The EPR-active nitroxide group of 16-DSA, on the other hand, resides near the end of the fatty acids' hydrocarbon tail. When the fatty acid is bound to the protein, this tail region is located close to that end of the hydrophobic binding channel, through which the fatty acid entered the binding site. Hence, the spatial distribution of 16-DSA is representative for the distribution of these entry points.

We found that the anchor points are asymmetrically distributed in the rigid interior of the protein as predicted by the crystal structure. In contrast, the entry points are distributed symmetrically on the protein's surface. This was attributed to a large conformational flexibility in solution which facilitates the uptake and release of the guest molecules. Furthermore, the rigidifying effect of ionic

Submitted February 10, 2011, and accepted for publication March 25, 2011.

*Correspondence: dariush.hinderberger@mpip-mainz.mpg.de

Matthias J. N. Junk's present address is Department of Chemical Engineering, University of California, Santa Barbara, CA.

Editor: David D. Thomas.

0006-3495/11/05/2293/9 $2.00

doi: 10.1016/j.bpj.2011.03.050

liquids as cosolvents on the solution structure was also revealed in such an approach (14).

Though the coarsened view on the protein by DEER spectroscopy helped in visualizing general structural motifs, the structural information, in the case of seven fatty acid binding sites, is limited to the analysis of the huge number of 21 distances. Hence, we sought for an opportunity to expand the breadth of the EPR approach to reveal additional, more detailed, and simplified structural data.

In addition to fatty acids, HSA binds and transports a large variety of endogenous compounds and drugs. Most drugs are bound in two distinct binding sites located in subdomains IIA and IIIA of the protein (24,25), which overlap with fatty acid binding sites 2 and 3/4 (26,27). Among the endogenous ligands, hemin, bilirubin, and tyroxine are the most important. Hemin and bilirubin bind to subdomain IB (fatty acid site 1) (28–30) whereas thyroxine binds to subdomain IIA (fatty acid site 7) (31).

Hemin is a particularly interesting ligand for EPR studies because it contains a paramagnetic Fe^{3+} central ion, which is complexed by a porphyrin derivative. It fits snugly into the hydrophobic cavity of the protein in subdomain IB with its two propionate groups interacting with basic side-chain residues of the protein (28). In that sense, its binding mode resembles that of fatty acids. Because hemin exhibits a higher affinity to the protein binding site than the fatty acids, the addition of one equivalent of hemin is sufficient to quantitatively replace the fatty acid bound to site 1. Note that HSA only provides one distinct binding site for hemin whereas six further binding sites remain for the complexation of fatty acids. The crystal structure PDB 1O9X of HSA, cocrystallized with hemin and myristic acid, is shown in Fig. 1 *A* (28).

The high-spin Fe^{3+} ion of hemin(chloride) possesses an electron spin of $S = 5/2$ (32), which leads to a substantially broadened EPR spectrum (see Fig. S1 in the Supporting Material). However, it can easily be substituted by a variety of transition metal ions. Cu^{2+} ($S = 1/2$) is the ion of choice for EPR applications, because its spectra exhibit comparably narrow spectral widths. Its relatively high spectral density makes Cu^{2+} a suitable probe for DEER distance measurements (33–36).

By the addition of Cu(II) protoporphyrin IX (replacing hemin) and 16-doxyl stearic acid (16-DSA, replacing myristic acid) to HSA (Fig. 1 *B*), a self-assembled ternary system is obtained that allows a structural characterization of the protein by EPR spectroscopy (Fig. 2). (Note that 16-DSA probes the entry points of the FA binding sites in the protein. These parts of the protein were identified to differ significantly from the crystal structure, triggering us to focus on this particular spin probe in this study to gain more detailed indications for a deviation of the crystallographic protein structure and its EPR-derived structure in solution.) The spectral separation of the contributions from the copper ion and the nitroxide radicals (see Fig. 3) opens up the possibility to solely retrieve distances between the Cu^{2+} ion in the center of the porphyrin and the nitroxide groups of the fatty acids. This results in a substantial simplification of the spectral analysis as the total number of distances probed is significantly reduced from 21 (FA-FA) to six (Cu(II)-FA). These six distances range from 2.4 nm to 4.3 nm as derived from the crystal structure (Fig. 2). Hence, they are well in the distance regime that can be accessed by DEER.

Moreover, the fraction of Cu^{2+} spins that can be excited by a single microwave pulse possesses a defined orientation with respect to the external magnetic field. Due to this orientation selection, not only information about the spin-spin distance but also information about the relative orientation of the spin-spin connecting vector with respect to the molecular frames of the paramagnetic centers is accessible (38,39).

Orientation-selective DEER spectroscopy is an emerging field in magnetic resonance. It requires the **g** anisotropy of at least one of the paramagnetic centers to be resolved. For nitroxides, a full resolution is only provided at high magnetic

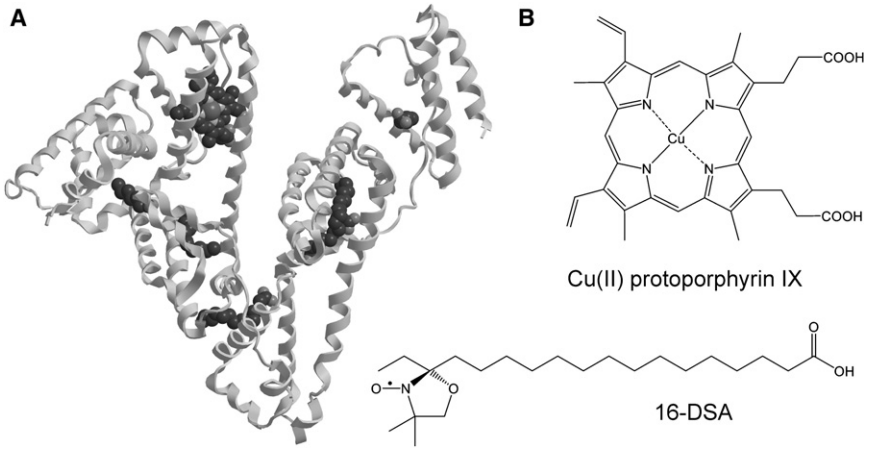

FIGURE 1 (*A*) Crystal structure (PDB 1O9X) of HSA co-crystallized with hemin and six myristic acid molecules (28). (*B*) Chemical structure of the EPR active substitutes for hemin and myristic acid, Cu(II) protoporphyrin IX, and 16-DSA.

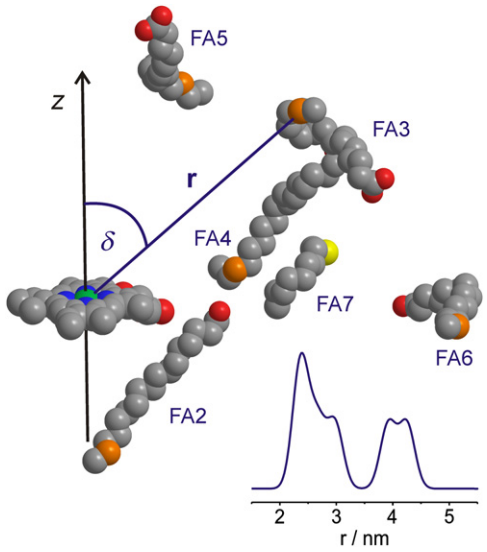

FIGURE 2 Relative positions of Cu(II) protoporphyrin IX and the stearic acid molecules in the protein. The structural model was obtained by inserting hemin into the crystal structure PDB 1E7I of HSA complexed with seven stearic acid molecules (5). The C-16 positions of the fatty acids (FA) and the last resolved carbon atom of stearic acid in site 7 are highlighted in light colors. The structural relationship between Cu(II) and the C-16 position of the stearic acids is sufficiently described by the distance and the angle δ between the connecting vector and the z axis of the molecular Cu(II) frame. (*Inset*) The expected distance distribution is shown assuming Gaussian peaks with $\sigma = 0.14$ nm. The methylene chain of the fatty acid in site 7 was linearly extrapolated to its C-16 position.

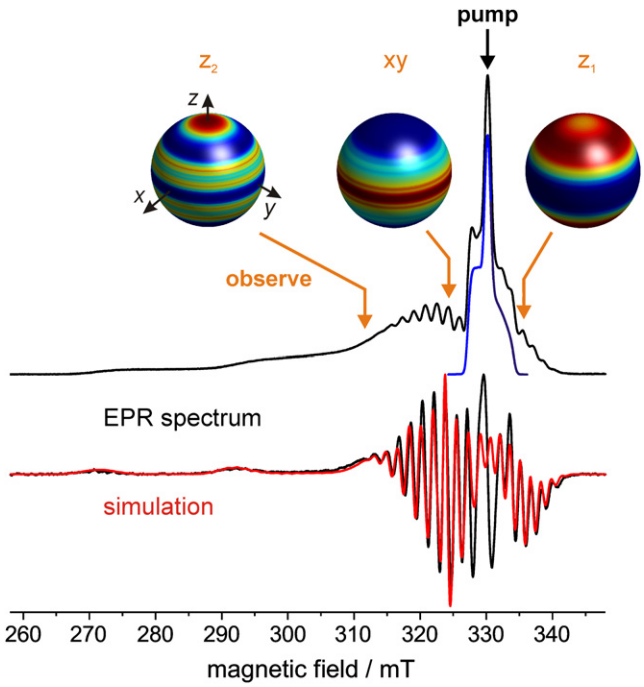

FIGURE 3 Electron-spin echo detected EPR absorption spectrum of HSA complexed with 1 eq. Cu(II) protoporphyrin IX and 1 eq. 16-DSA at 10 K (*top*). The nitroxide contribution to this spectrum was approximated by a 1:2 mixture of HSA and 16-DSA at 50 K and is also shown. The difference spectrum was pseudomodulated and simulated (*bottom*). The spectral parameters retrieved by the simulation were used to calculate the Cu(II) orientations that are excited by a 32 ns pulse at a certain spectral position. The frequency of the pump pulse in the DEER experiment was kept at the maximum of the nitroxide spectrum and at the center of the resonator mode whereas the position of the observer pulse was varied within the copper spectrum. The orientation selection for the observer positions is displayed in unit sphere plots. High excitation efficiencies are indicated by warm colors.

fields ($\nu_{mw} \geq 95$ GHz), which allows spin-pair geometries to be accessed (40–44). Limited orientational information on nitroxides can also be accessed at X-band (ν_{mw} ~9–10 GHz) because a variation of the observer pulse position in the low field part of the spectrum slightly affects the orientation of the excited spins (45,46).

Transition metals with significantly larger **g** anisotropy, however, give rise to a strong angular selection already at low magnetic fields. Copper-nitroxide distances and orientations were accessed for terpyridine and porphyrin model complexes (33,47), and even copper-copper distances could be estimated for several biological systems (33,35,48,49).

In orientation-selective DEER, a direct conversion of dipolar data into distance distributions is not possible because the orientation dependence of the dipolar data is, a priori, unknown. In recent years, several sophisticated methods were developed for the analysis of orientation selection in DEER (40,44,46,50). Here, we introduce a simplified method to calculate angular dipolar DEER data, when only one spin of the spin pair (here Cu(II)) is predominantly responsible for the orientation selection.

This article is organized as follows: The next section contains details about the preparation of the biological self-assembled system, the orientation-selective DEER experiment, and its analysis. The latter is briefly discussed in Results and Discussion before the spectroscopic data are presented and compared to the calculated spectra based on the crystal structure. The apparent discrepancy of the two datasets and its implication for the functional protein structure in solution is discussed in light of previous findings.

MATERIALS AND METHODS

Materials

Nondenaturated human serum albumin (HSA, >95%; Calbiochem, San Diego, CA), hemin(chloride) (>98%; Carl Roth, Karlsruhe, Germany), Cu(II) protoporphyrin IX (Frontier Scientific, Logan, UT), 16-doxylstearic acid (16-DSA; Sigma-Aldrich, St. Louis, MO), and glycerol (87 wt %; Fluka Chemical, Milwaukee, WI) were used as received. 16-DSA was partly reduced to the EPR-inactive hydroxylamine (16-rDSA) by addition of phenylhydrazine (97%; Sigma-Aldrich) (13).

Sample preparation

A quantity of 0.2 M phosphate-buffered solutions of pH 6.4 with and without 2 mM HSA and 6.7 mM solutions of 16-DSA and Cu(II) protoporphyrin IX in 0.1 M KOH were prepared. These stock solutions were mixed

in the appropriate ratios to obtain HSA complexes with 1 eq. Cu(II) protoporphyrin IX, 1 eq. 16-DSA, and up to 4 eq. of 16-rDSA in a 100 mM phosphate buffer solution of pH 7.4. This method provides for isolated spin pairs in combination with a varying total occupation of the fatty acid binding sites. The combined concentration of 16-DSA and 16-rDSA was kept constant at 2 mM. A quantity of 20 vol % glycerol was added to the final solutions to prevent crystallization upon freezing. The solutions were filled into 3 mm O.D. quartz tubes and shock-frozen in $N_2(l)$ cooled *iso*-pentane (below –100°C).

Electron-spin-echo-detected spectrum and simulation

Electron-spin-echo-detected spectra were acquired using the primary echo sequence $\pi/2$-τ-π-τ-echo with $\tau = 200$ ns. The temperature was set to 10 K by cooling with a closed cycle cryostat (ARS AF204, customized for pulse EPR; ARS, Macungie, PA). The nitroxide contribution to this combined copper/nitroxide spectrum was partly removed by subtraction of a nitroxide spectrum from a 1:2 mixture of HSA and 16-DSA. The residual spectrum was pseudomodulated with a modulation amplitude of 1 mT (51) and simulated with a home-written MATLAB (The MathWorks, Natick, MA) program, which utilizes the rigid limit routine of the EASYSPIN software package for EPR (52,53). Collinear uniaxial **g** and **A** tensors and a natural isotopic composition of Cu (69.2% ^{63}Cu, 30.8% ^{65}Cu) were assumed.

Cu(II)-nitroxide DEER measurements

Dipolar time evolution data were obtained at X-band frequencies (9.2–9.4 GHz) with an Elexsys 580 spectrometer (Bruker BioSpin, Rheinstetten, Germany) equipped with a Flexline split-ring resonator ER4118X_MS3 (Bruker Optics) using the four-pulse DEER experiment with the pulse sequence $\pi/2(\nu_{obs})$-τ_1-$\pi(\nu_{obs})$-(τ_1+t)-$\pi(\nu_{pump})$-(τ_2-t)-$\pi(\nu_{obs})$-τ_2-echo (16,17). The dipolar evolution time t was varied whereas $\tau_2 = 2.5$ μs and τ_1 were kept constant. Proton modulation was averaged by addition of eight time traces of variable τ_1, starting with $\tau_{1,0} = 200$ ns and incrementing by $\Delta\tau_1 = 8$ ns (54). The resonator was overcoupled to $Q \approx 100$. The frequency of the pump pulse ν_{pump} was kept at the maximum of the nitroxide spectrum and at the center of the resonator mode whereas the position of the observer pulse was varied in the copper spectrum (compare to Fig. 3). The observer pulse lengths were 32 ns for both $\pi/2$ and π pulses and the pump pulse length was 12 ns. The raw time domain DEER data were processed with the program package DeerAnalysis2008 (55). Intermolecular contributions were removed by division by an exponential decay with a fractal dimension of $d = 3.8$. The deviation from $d = 3.0$ originates from excluded volume effects due to the size of the protein (13,56). The resulting time traces were normalized to $t = 0$.

Analysis of DEER data

The spectral parameters of the copper spectrum were used to calculate the orientation selection at different observer pulse positions (EASYSPIN routine Orisel). These orientational weights $\lambda(\theta)$ were implemented in a home-written MATLAB program, which simulated DEER time-domain data and frequency spectra based on crystallographic data. In crystal structure PDB 1O9X, HSA is cocrystallized with hemin and six myristic acid molecules (28). In PDB 1E7I, HSA is cocrystallized with seven stearic acid molecules (5). The distances and relative orientations between the central atom of the porphyrin complex (representing Cu^{2+}) and the C-16 positions of the fatty acids (as an approximation for the free nitroxide electron) were obtained by merging the two crystal structures in one common coordinate system.

The orientational relationship between porphyrin and fatty acid is expressed by the angle δ between the connecting vector **r** (Cu(II)-C-16) and the z axis of the molecular Cu(II) frame. The C-16 position of the stearic acid in site 7 was obtained by linear extrapolation of the aliphatic alkyl chain. Six distance-angle pairs (r, δ) were obtained: (2.36 nm, 64.7°), (2.98 nm, 56.2°), (2.38 nm, 85.7°), (4.25 nm, 73.2°), (3.93 nm, 88.5°), and (2.67 nm, 75.8°). The infinitesimal sharp distances were broadened by a Gaussian distribution with $\sigma = 0.14$ nm. Each distance peak was divided into 40 equally spaced contributions ($\Delta r = 0.05$ nm), which were weighted according to the Gaussian distribution.

Because only copper exhibits a pronounced orientation selection, the molecular coordinate frame of Cu^{2+} served as reference frame. Ten-thousand dipolar frequencies were calculated for each distance contribution of each distance-angle pair, originating from an array of 100 × 100 orientations of the magnetic field vector in the unit sphere (57),

$$\omega(r,\theta) = \frac{\mu_0}{4\pi\hbar}\frac{g_N g_{Cu}\beta_e^2}{r^3}\left(3\cos^2\theta - 1\right). \quad (1)$$

The value θ defines the angle between the spin-spin connecting vector and magnetic field vector. The effective g_{Cu} value for each orientation of the magnetic field vector was obtained by (57)

$$g(\theta) = \left(g_\perp^2 \sin^2\theta + g_\parallel^2 \cos^2\theta\right)^{1/2}. \quad (2)$$

The dipolar frequencies were multiplied with the orientational weight for the respective magnetic field orientation $\lambda(\theta)$ and by $\sin\theta$. These frequency contributions were added to generate dipolar spectra (40). The DEER time-domain data were independently calculated by (57)

$$V(r,t) = 1 - \int_0^{\pi/2} \sin(\theta)\,\lambda(\theta)[1 - \cos(\omega(\theta)t)]d\theta. \quad (3)$$

To shorten the calculation time, only magnetic field vector orientations with weights >1% and contributions to the Gaussian distance peaks with weights >5% of the maximum values were considered. For six distances, the calculation time was <30 min.

RESULTS AND DISCUSSION

In orientation-selective DEER, a method for the direct conversion of the dipolar data into a distance distribution has not yet been developed. Existing methods utilize structural models to obtain the distance and mutual spin orientations of the dipolar coupled electron spins (40,44,46,50). The orientation selection of both dipolar coupled electron spins A and B is calculated and their mutual orientation accounted for by Euler angle transformation of the molecular frame of spin B in the molecular frame of spin A. The resulting excitation pattern is then related to the mutual orientation of spin A to the spin-spin connecting vector. This allows the dipolar couplings to be calculated and to be fitted to the experimental time-domain data or its Fourier transform.

This thorough methodology completely describes the mutual orientation of the whole spin system. However, a defined relationship between both spins does not always exist. In the self-assembled biological system in this study, the nitroxide moieties of the spin-labeled fatty acids assume a large range of orientations in the binding cavity. The lack of a defined orientational order was confirmed by field-swept DEER measurements (56). Thus, the orientation

selection is dominated by the transition metal ion, which exhibits a fixed position with respect to the spin-spin vector and possesses substantially larger **g** anisotropy.

In this case, only the orientation-selective excitation of the copper-centered electron spins needs to be considered. The relative fractions of excited Cu(II) spins at each angular orientation $\lambda(\theta)$ with respect to the external magnetic field can be readily calculated for each position in the EPR spectrum (52).

The lengths r of the spin-spin vectors and their angles to the Cu(II) molecular z axis δ were obtained from the crystal structure (Fig. 2). The position of the electron spin of the nitroxide was approximated by the C-16 position of the fatty acid. The relative positions of the nitroxides to the Cu(II) porphyrin are fully described by r and δ due to the axial symmetry of the Cu(II) molecular frame. The infinitesimal sharp distances r were broadened by a Gaussian distribution.

Powder averaging was achieved by varying the orientation of the external magnetic field in an angular grid of 10,000 orientations. For each orientation, the angle θ between the magnetic field and the spin-spin vector was determined and the dipolar frequency was calculated. Dipolar spectra were then obtained by weighting the dipolar frequencies by the fraction of excited Cu(II) spins and subsequent summation for all orientations. The full analysis method is explained in detail in Materials and Methods.

A typical EPR spectrum of HSA complexed with Cu(II) protoporphyrin IX and 16-DSA is displayed in Fig. 3 (*top*). The sharp maximum of the spectrum stems from the nitroxide moieties of the spin-labeled fatty acids, as visualized separately in blue. The spectral contribution from the paramagnetic Cu(II) ions alone was approximated by subtraction of the nitroxide contribution from the overall spectrum. A spectral simulation (*red*) yielded uniaxial EPR parameters $g_\perp = 2.053$, $g_\parallel = 2.194$, $A_\perp(^{63}\mathrm{Cu}) = 58.8$ MHz, $A_\parallel(^{63}\mathrm{Cu}) = 616$ MHz, and $\mathbf{A}(^{65}\mathrm{Cu}) = 1.07 \times \mathbf{A}(^{63}\mathrm{Cu})$, further superhyperfine couplings to four strongly coupled ^{14}N atoms with magnitudes $A_\perp(^{14}\mathrm{N}) = 50.4$ MHz and $A_\parallel(^{14}\mathrm{N}) = 37.8$ MHz. These values correspond well with reported values on similar Cu(II) porphyrin systems (58). The extracted parameters are used to calculate and predict the orientation selection of the Cu(II) ions at any position within the spectrum (52).

In the DEER measurements, the pump pulse was positioned at the maximum of the nitroxide spectrum where all orientations contribute significantly. This minimizes orientation selection from these spins and furthermore provides for a large fraction of pumped spins. The position of the observer pulse was varied within the copper spectrum to excite spin packages with different orientations. Orientational unit spheres for three typical observer pulse positions are depicted in Fig. 3.

An exclusive excitation of spins along the unique axis of the distorted octahedral Cu(II) frame is only possible at very low magnetic field positions. However, observer pulse position z_2 already exhibits a frequency offset of 500 MHz to the pump pulse position at the spectral maximum, which severely decreases the signal/noise ratio as both the flank of the resonator mode is approached and the spectral density is decreased. Nonetheless, Bode et al. (47) and Lovett et al. (50), performing DEER measurement on comparable Cu(II) porphyrins, chose this option to achieve a significant fractions of Cu(II) spins with desired orientations along z. Luckily, a comparable orientation selection is also possible at the high field flank of the spectrum (position z_1) due to a strong hyperfine coupling of the unpaired electron to the nuclear spin of the Cu^{2+} ion. As depicted in Fig. S2, both observer pulse positions give rise to similar DEER spectra—with a substantially increased signal/noise ratio for position z_1.

The DEER time-domain data and frequency spectra for observer pulse positions xy and z_1 are displayed in Fig. 4. Up to six fatty acids need to be added to one HSA molecule to occupy all remaining binding sites in the protein (one FA binding site is blocked by Cu(II) protoporphyrin IX). However, as we have shown for the self-assembled HSA/FA system, the interaction of more than two paramagnetic moieties in the protein leads to artifacts in the dipolar spectra (compare to Fig. S3) (56). To allow for a quantitative interpretation of the data, it is mandatory to limit the number of paramagnetic moieties per protein to two (13). In this study a protein molecule contains one Cu^{2+} spin and one EPR-active 16-DSA molecule on average. The degree of

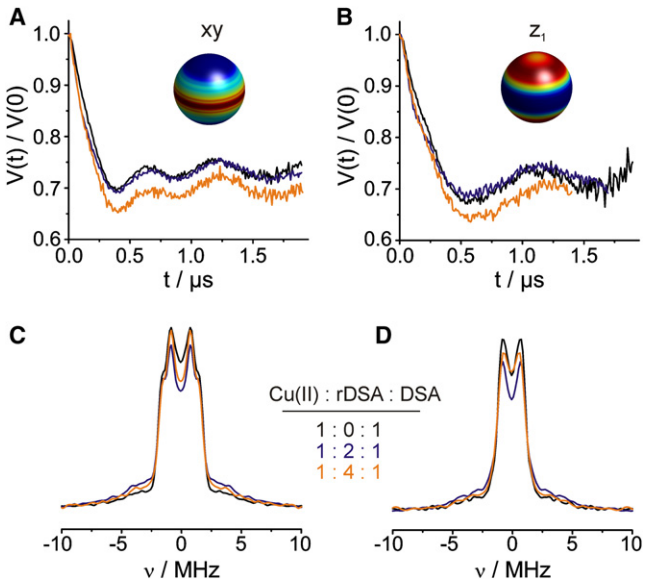

FIGURE 4 Background-corrected DEER time-domain data (*A* and *B*) and dipolar spectra (*C* and *D*) of HSA complexed with 1 eq. of Cu(II) protoporphyrin IX, 1 eq. of 16-DSA, and varying amounts of 16-rDSA. Observer pulses were applied at field positions exciting Cu(II) orientations either (*A* and *C*) predominantly in the *xy* plane of the porphyrin ring (*position xy*) or (*B* and *D*) outerdiagonal elements toward the molecular z axis of Cu(II) (*position* z_1).

FA loading can be varied by the addition of diamagnetic fatty acids (16-rDSA), which compete with 16-DSA for a binding site without giving rise to an EPR signal. Continuous wave (CW) EPR spectra reveal a nearly quantitative complexation of fatty acids up to a HSA/fatty acid ratio of 1:5 (Fig. S2) and ensure that all FA binding sites are readily occupied by the DSA-derivatives under the experimental conditions in this study.

Well-defined dipolar modulations are observed in the DEER time-domain data (Fig. 4). These modulations stem from dipolar couplings of spin pairs with a single dominating distance. This is somewhat surprising given the large distribution of distances that is suggested by the crystal structure (Fig. 2). However, these results are in agreement with previous EPR findings on the fatty acid distribution in the protein (13). Experimental distance distributions between 16-DSA molecules in the binding sites of the protein revealed an overwhelmingly dominant distance peak at 3.6 nm in strong contrast to the complex distance distribution predicted by the crystallographic data. The nitroxide moiety of 16-DSA is located at the tail of the methylene chain of the FA, which is located near the entry points of the FA binding sites. This dominating distance strongly indicates a very symmetric distribution of these entry points on the protein surface. Here, the dipolar data contain information about the distances between Cu(II) protoporphyrin IX and the entry points of the FA binding sites (represented by 16-DSA). The repeated occurrence of a dominating distance in a new reference frame supports the conclusion of a symmetric distribution of the entry points.

Furthermore, the dipolar data do not change significantly when the protein is loaded with varying amounts of fatty acids, i.e., when the occupation of FA binding sites is varied. This behavior has already been observed when only fatty acids were added to HSA. A strong dependence of the degree of loading would be expected when binding sites with a higher affinity for fatty acids are populated before the low-affinity binding sites. However, a consecutive population of different binding sites cannot be excluded under the premise that the entry points of all binding sites exhibit a similar distance to the Cu(II) ion as suggested by the DEER data. We note that a high degree of FA loading caused a slight broadening of the dipolar modulations when probing the distances between 16-DSA.

The almost complete absence of a broadening in this study could be due to far fewer spin-pair interactions even in the case of full loading. The interaction of a Cu(II) ion with the doxyl reporters of the fatty acids results in six dipolar interactions whereas FA-FA interactions can lead to 21 potential distances. Further, the Cu(II) ion is located in a rigid framework which keeps its position fixed in the protein. On the contrary, the aliphatic fatty acid chains experience considerable degrees of freedom even in a confined binding pocket.

Although the degree of FA loading does not influence the DEER data, a variation of the observer position in the Cu(II) spectrum causes significant changes. Indeed, a pronounced orientation selection is observed when comparing the time traces in Fig. 4. At the *xy* position of the observer pulse, the dipolar modulations oscillate with a frequency twice that at the z_1 position. At this position, the dipolar contribution from angles $\theta = 0^\circ$ is far more pronounced than in a Pake pattern of a disordered system with no orientational selection. At the same time, the dipolar singularities at $\theta = 90^\circ$ are the only pronounced feature of the dipolar spectrum at an observer position z_1, as contributions from $\theta = 0^\circ$ are almost absent.

The measured dipolar data are compared to data calculated from the crystal structure in Fig. 5 (representation in the time domain in Fig. S4), assuming full occupation of all binding sites. The dominating feature of the measured spectra is approximately reproduced by the calculated data regarding both strength and orientation of the dipolar coupling. The strong contribution from dipolar angles $\theta = 0^\circ$ at observer pulse position *xy* is clearly visible in the calculated spectra and even more pronounced in the measured data. However, strong dipolar couplings due to small distances at ~2.5 nm (frequency range 2.5–5 MHz) are almost entirely absent in the measured DEER data. In this frequency region, the calculated spectra inferred from the crystal structure exhibit significantly higher spectral density.

Spectral simulations of the measured dipolar spectra yield information on distance and relative orientation of the

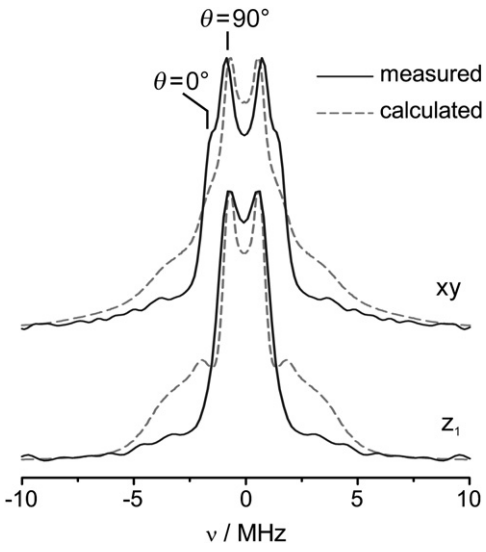

FIGURE 5 Recorded dipolar spectra of HSA complexed with 1 eq. Cu (II) protoporphyrin IX, 4 eq. 16-rDSA, and 1 eq. 16-DSA (*solid/black lines*) and calculated Pake patterns (*dashed/gray lines*) for observer pulse positions *xy* and z_1. The calculated Pake patterns are obtained assuming full occupation of all fatty acid binding sites (2–7). Specific angular orientations $\theta = 0^\circ$ and $\theta = 90^\circ$ of the dominant dipolar contribution are indicated in the spectra.

dominant dipolar contribution. Interestingly, this contribution can be reproduced by a single dipolar interaction between Cu(II) and a nitroxide group (see Fig. 6 *A*, and representation in the time domain in Fig. S5). The qualitative description of Fig. 5 in the last paragraph is confirmed by the quantitative simulation, which yields a distance $r = 3.85$ nm and an angular orientation $\delta = 90 \pm 10°$ (Fig. S6). Note that the contributions from $\theta = 0°$ even exceed the maximum achievable contribution at the given Cu(II) orientation selection for the *xy* observer position. This increase of the orientation selection may be related to an additional slight preferential orientation of the nitroxide spin labels, which is not accounted for in the spectral analysis.

The obtained parameters correspond to a circle in the porphyrin plane, which is depicted graphically in Fig. 6 *B*. Indeed, a particular circular position almost coincides with the C-16 position of the stearic acid in binding site 6 ($r = 3.82$ nm, $\delta = 88.1°$). This site was previously assigned a low-affinity binding site for fatty acids (26,27).

Yet, the observed dipolar coupling cannot stem from a single dipolar contribution (as, e.g., between hemin and the fatty acid in binding site 6). As inferred by CW EPR spectroscopy, >99% of the fatty acids are complexed by a Cu(II) protoporphyrin IX-loaded HSA molecule even at HSA-fatty acid ratios as high as 1:5 (Fig. S2). This corresponds to a full occupation of five out of six available binding sites of the protein. The CW data hence suggest that the strong binding affinity of the protein toward multiple fatty acids is not altered by a simultaneously bound hemin-analog molecule.

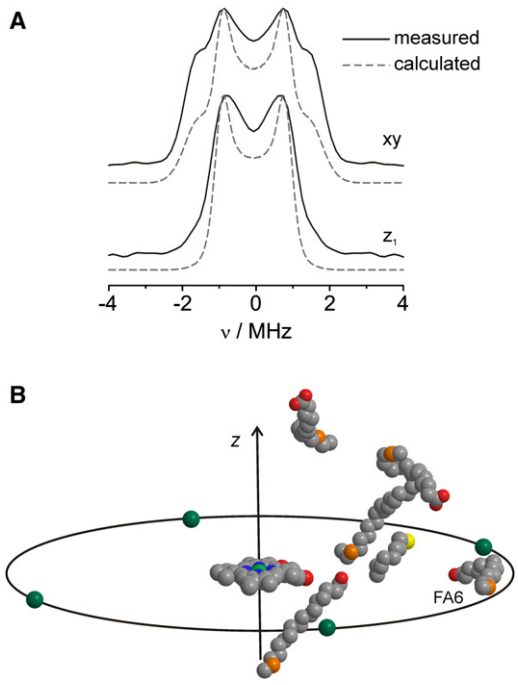

FIGURE 6 Predominant dipolar contribution in the measured DEER spectra. (*A*) Measured dipolar spectra of HSA complexed with 1 eq. of Cu(II) protoporphyrin IX and 16-DSA (*solid/black lines*) and best spectral fits based on a single dipolar coupling (*dashed/gray lines*). Best fits are obtained if the coupled electron spin is assumed to be placed in the extended *xy* plane of the porphyrin ring ($\delta = 90°$) with a distance of $r = 3.85$ nm to Cu(II). (*B*) Structural relation of the dominant DEER contribution to the fatty acid positions of the crystal structure. Potential positions for the dipolar coupled electron spin are indicated by a circle that is located close to the C-16 position of the stearic acid in site 6.

Hence, it is far more reasonable that the well-defined dominant dipolar coupling is due to various Cu(II)-nitroxide spin pairs with similar distances and an orientation of the spin-spin vectors close to the porphyrin plane. This is accounted for by a symmetric distribution of the fatty acids tails and the entries to the fatty acid binding sites in the protein. Hence, this study corroborates the structural assumption of our recent EPR study that the flexible protein surface allows for a symmetric distribution of the entry points of the fatty acid binding sites (13). This assumption is also supported by the fact that the found distance of 3.85 nm between Cu(II) and the 16-DSA molecules is close to the dominating 16-DSA-16-DSA distance of 3.6 nm.

As inferred from the crystal structure (28), the global structure of HSA resembles an ellipsoid or a uniaxially compressed sphere. The pronounced orientation selection in our Cu(II)-nitroxide DEER data reflects the fact that the *xy* plane of the porphyrin ring is roughly aligned along the flattened side of the protein. Hence, all spin-spin vectors between Cu(II) and the fatty acids are predominantly located at angles close to $\delta = 90°$ (compare to calculated angles from the crystal structure in the Materials and Methods).

We note that Cu(II) porphyrin does not only serve as EPR probe but also blocks the fatty acid binding site 1. When adding two equivalents of paramagnetic 16-DSA, nitroxide-nitroxide distances can be accessed. The obtained DEER-derived distance distributions with only six accessible FA binding sites hardly deviate from the distributions from 16-DSA in all seven FA binding sites (Fig. S7). In contrast, the loss of binding site 1 causes the crystal structure derived distance distributions to exhibit marked differences. This is further indication for a rather symmetric distribution of the entry points to the binding sites in the protein even when a porphyrin molecule is bound. This highlights the strong conformational flexibility in particular of the surface of HSA, which seems to be the foundation for the excellent transport, uptake, and release properties of HSA.

CONCLUSIONS

Orientation-selective DEER measurements between the hemin substitute Cu(II) protoporphyrin IX and spin-labeled stearic acids (16-DSA, representing the entry points of the FA binding sites of HSA) reveal one dominant dipolar contribution and a strong orientation selection. Although the observed orientation selection in the dipolar spectra

reflects the overall flattened shape of the protein, the finding of one dominant dipolar contribution and hence Cu(II)-nitroxide distance indicates a symmetric distribution of the binding site entry points on the protein's surface. This symmetric distribution may enhance the access of the protein by fatty acids and thus facilitate the uptake and release of fatty acids and potentially other (small) guest molecules even when a larger hemin-analog molecule is rather rigidly placed in a central region of HSA. Furthermore, the conformational flexibility at the surface of the protein as probed by the entry point distribution is retained even with a porphyrinoid molecule bound.

SUPPORTING MATERIAL

Seven figures are available at http://www.biophysj.org/biophysj/supplemental/S0006-3495(11)00408-5.

We thank Gunnar Jeschke, ETH Zurich, for many helpful discussions as well as for providing a MATLAB program for the analysis of orientation-selective DEER of nitroxide spin pairs at high magnetic fields (35). We thank Christian Bauer for technical support.

M.J.N.J. gratefully acknowledges financial support from the Fonds der Chemischen Industrie, from the Graduate School of Excellence "Materials Science in Mainz," and from a Feodor-Lynen fellowship from the Alexander von Humboldt-Foundation.

REFERENCES

1. Peters, T. 1995. All About Albumin: Biochemistry, Genetics and Medical Applications. Academic Press, San Diego, CA.
2. Carter, D. C., and J. X. Ho. 1994. Structure of serum albumin. *Adv. Protein Chem.* 45:153–203.
3. Spector, A. A. 1975. Fatty acid binding to plasma albumin. *J. Lipid Res.* 16:165–179.
4. Hamilton, J. A., D. P. Cistola, …, D. M. Small. 1984. Interactions of myristic acid with bovine serum albumin: a ^{13}C NMR study. *Proc. Natl. Acad. Sci. USA.* 81:3718–3722.
5. Bhattacharya, A. A., T. Grüne, and S. Curry. 2000. Crystallographic analysis reveals common modes of binding of medium and long-chain fatty acids to human serum albumin. *J. Mol. Biol.* 303:721–732.
6. Fasano, M., S. Curry, …, P. Ascenzi. 2005. The extraordinary ligand binding properties of human serum albumin. *IUBMB Life.* 57:787–796.
7. Curry, S., H. Mandelkow, …, N. Franks. 1998. Crystal structure of human serum albumin complexed with fatty acid reveals an asymmetric distribution of binding sites. *Nat. Struct. Biol.* 5:827–835.
8. Curry, S., P. Brick, and N. P. Franks. 1999. Fatty acid binding to human serum albumin: new insights from crystallographic studies. *Biochim. Biophys. Acta.* 1441:131–140.
9. Henzler-Wildman, K., and D. Kern. 2007. Dynamic personalities of proteins. *Nature.* 450:964–972.
10. Lange, O. F., N.-A. Lakomek, …, B. L. de Groot. 2008. Recognition dynamics up to microseconds revealed from an RDC-derived ubiquitin ensemble in solution. *Science.* 320:1471–1475.
11. Karush, F. 1950. Heterogeneity of the binding sites of bovine serum albumin. *J. Am. Chem. Soc.* 72:2705–2713.
12. Karush, F. 1954. The interaction of optically isomeric dyes with human serum albumin. *J. Am. Chem. Soc.* 76:5536–5542.
13. Junk, M. J. N., H. W. Spiess, and D. Hinderberger. 2010. The distribution of fatty acids reveals the functional structure of human serum albumin. *Angew. Chem. Int. Ed. Engl.* 49:8755–8759.
14. Akdogan, Y., M. J. N. Junk, and D. Hinderberger. 2011. Effect of ionic liquids on the solution structure of human serum albumin. *Biomacromolecules.* 12:1072–1079.
15. Milov, A. D., K. M. Salikhov, and M. D. Shirov. 1981. Application of ENDOR in electron-spin echo for paramagnetic center space distribution in solids. *Fiz. Tverd. Tela.* 23:975–982.
16. Pannier, M., S. Veit, …, H. W. Spiess. 2000. Dead-time free measurement of dipole-dipole interactions between electron spins. *J. Magn. Reson.* 142:331–340.
17. Jeschke, G., M. Pannier, and H. W. Spiess. 2000. Double electron-electron resonance. *In* Biological Magnetic Resonance: Distance Measurements in Biological Systems by EPR. L. J. Berliner, G. R. Eaton, and S. S. Eaton, editors. Kluwer Academic, New York. 493–511.
18. Jeschke, G. 2002. Distance measurements in the nanometer range by pulse EPR. *ChemPhysChem.* 3:927–932.
19. Jeschke, G. 2002. Determination of the nanostructure of polymer materials by electron paramagnetic resonance spectroscopy. *Macromol. Rapid Commun.* 23:227–246.
20. Hinderberger, D., O. Schmelz, …, G. Jeschke. 2004. Electrostatic site attachment of divalent counterions to rodlike ruthenium(II) coordination polymers characterized by EPR spectroscopy. *Angew. Chem. Int. Ed. Engl.* 43:4616–4621.
21. Schiemann, O., and T. F. Prisner. 2007. Long-range distance determinations in biomacromolecules by EPR spectroscopy. *Q. Rev. Biophys.* 40:1–53.
22. Jeschke, G., and Y. Polyhach. 2007. Distance measurements on spin-labeled biomacromolecules by pulsed electron paramagnetic resonance. *Phys. Chem. Chem. Phys.* 9:1895–1910.
23. Martin, R. E., M. Pannier, …, H. W. Spiess. 1998. Determination of end-to-end distances in a series of TEMPO diradicals of up to 2.8 nm length with a new four-pulse double electron-electron resonance experiment. *Angew. Chem. Int. Ed.* 37:2834–2837.
24. He, X. M., and D. C. Carter. 1992. Atomic structure and chemistry of human serum albumin. *Nature.* 358:209–215.
25. Curry, S. 2009. Lessons from the crystallographic analysis of small molecule binding to human serum albumin. *Drug Metab. Pharmacokinet.* 24:342–357.
26. Simard, J. R., P. A. Zunszain, …, J. A. Hamilton. 2005. Locating high-affinity fatty acid-binding sites on albumin by x-ray crystallography and NMR spectroscopy. *Proc. Natl. Acad. Sci. USA.* 102:17958–17963.
27. Simard, J. R., P. A. Zunszain, …, S. Curry. 2006. Location of high and low affinity fatty acid binding sites on human serum albumin revealed by NMR drug-competition analysis. *J. Mol. Biol.* 361:336–351.
28. Zunszain, P. A., J. Ghuman, …, S. Curry. 2003. Crystal structural analysis of human serum albumin complexed with hemin and fatty acid. *BMC Struct. Biol.* 3:6. 10.1186/1472-6807-1183-1186.
29. Zunszain, P. A., J. Ghuman, …, S. Curry. 2008. Crystallographic analysis of human serum albumin complexed with 4Z,15E-bilirubin-IXα. *J. Mol. Biol.* 381:394–406.
30. Wardell, M., Z. M. Wang, …, D. C. Carter. 2002. The atomic structure of human methemalbumin at 1.9 Å. *Biochem. Biophys. Res. Commun.* 291:813–819.
31. Petitpas, I., C. E. Petersen, …, S. Curry. 2003. Structural basis of albumin-thyroxine interactions and familial dysalbuminemic hyperthyroxinemia. *Proc. Natl. Acad. Sci. USA.* 100:6440–6445.
32. Hoard, J. L. 1971. Stereochemistry of hemes and other metalloporphyrins. *Science.* 174:1295–1302.
33. Narr, E., A. Godt, and G. Jeschke. 2002. Selective measurements of a nitroxide-nitroxide separation of 5 nm and a nitroxide-copper separation of 2.5 nm in a terpyridine-based copper(II) complex by pulse EPR spectroscopy. *Angew. Chem. Int. Ed. Engl.* 41:3907–3910.
34. van Amsterdam, I. M. C., M. Ubbink, …, M. Huber. 2003. Measurement of a Cu-Cu distance of 26 Å by a pulsed EPR method. *Angew. Chem. Int. Ed. Engl.* 42:62–64.

35. Bund, T., J. M. Boggs, …, D. Hinderberger. 2010. Copper uptake induces self-assembly of 18.5 kDa myelin basic protein (MBP). *Biophys. J.* 99:3020–3028.

36. Yang, Z., M. Ji, and S. Saxena. 2010. Practical aspects of copper ion-based double electron-electron resonance distance measurements. *Appl. Magn. Reson.* 39:487–500.

37. Reference deleted in proof.

38. Larsen, R. G., and D. J. Singel. 1993. Double electron-electron resonance spin-echo modulation: spectroscopic measurement of electron spin pair separations in orientationally disordered solids. *J. Chem. Phys.* 98:5134–5146.

39. Maryasov, A. G., Y. D. Tsvetkov, and J. Raap. 1998. Weakly coupled radical pairs in solids: ELDOR in ESE structure studies. *Appl. Magn. Reson.* 14:101–113.

40. Polyhach, Y., A. Godt, …, G. Jeschke. 2007. Spin pair geometry revealed by high-field DEER in the presence of conformational distributions. *J. Magn. Reson.* 185:118–129.

41. Hertel, M. M., V. P. Denysenkov, …, T. F. Prisner. 2005. Pulsed 180-GHz EPR/ENDOR/PELDOR spectroscopy. *Magn. Reson. Chem.* 43 (Spec no):S248–S255.

42. Denysenkov, V. P., T. F. Prisner, …, M. Bennati. 2006. High-field pulsed electron-electron double resonance spectroscopy to determine the orientation of the tyrosyl radicals in ribonucleotide reductase. *Proc. Natl. Acad. Sci. USA.* 103:13386–13390.

43. Denysenkov, V. P., D. Biglino, …, M. Bennati. 2008. Structure of the tyrosyl biradical in mouse R2 ribonucleotide reductase from high-field PELDOR. *Angew. Chem. Int. Ed. Engl.* 47:1224–1227.

44. Savitsky, A., A. A. Dubinskii, …, K. Möbius. 2007. Orientation-resolving pulsed electron dipolar high-field EPR spectroscopy on disordered solids: I. Structure of spin-correlated radical pairs in bacterial photosynthetic reaction centers. *J. Phys. Chem. B.* 111:6245–6262.

45. Schiemann, O., P. Cekan, …, S. T. Sigurdsson. 2009. Relative orientation of rigid nitroxides by PELDOR: beyond distance measurements in nucleic acids. *Angew. Chem. Int. Ed. Engl.* 48:3292–3295.

46. Margraf, D., B. E. Bode, …, T. F. Prisner. 2007. Conformational flexibility of nitroxide biradicals determined by X-band PELDOR experiments. *Mol. Phys.* 105:2153–2160.

47. Bode, B. E., J. Plackmeyer, …, O. Schiemann. 2008. PELDOR measurements on a nitroxide-labeled Cu(II) porphyrin: orientation selection, spin-density distribution, and conformational flexibility. *J. Phys. Chem. A.* 112:5064–5073.

48. Kay, C. W. M., H. E. Mkami, …, R. W. Evans. 2007. Pulsed ELDOR determination of the intramolecular distance between the metal binding sites in dicupric human serum transferrin and lactoferrin. *J. Am. Chem. Soc.* 129:4868–4869.

49. Yang, Z., J. Becker, and S. Saxena. 2007. On Cu(II)-Cu(II) distance measurements using pulsed electron-electron double resonance. *J. Magn. Reson.* 188:337–343.

50. Lovett, J. E., A. M. Bowen, …, J. Harmer. 2009. Structural information from orientationally selective DEER spectroscopy. *Phys. Chem. Chem. Phys.* 11:6840–6848.

51. Hyde, J. S., M. Pasenkiewicz-Gierula, …, W. E. Antholine. 1990. Pseudofield modulation in EPR spectroscopy. *Appl. Magn. Reson.* 1: 483–496.

52. Stoll, S., and A. Schweiger. 2006. EasySpin, a comprehensive software package for spectral simulation and analysis in EPR. *J. Magn. Reson.* 178:42–55.

53. Stoll, S., and A. Schweiger. 2003. An adaptive method for computing resonance fields for continuous-wave EPR spectra. *Chem. Phys. Lett.* 380:464–470.

54. Jeschke, G., A. Bender, …, A. Godt. 2004. Sensitivity enhancement in pulse EPR distance measurements. *J. Magn. Reson.* 169:1–12.

55. Jeschke, G., V. Chechik, …, H. Jung. 2006. DeerAnalysis2006—a comprehensive software package for analyzing pulsed ELDOR data. *Appl. Magn. Reson.* 30:473–498.

56. Junk, M. J. N., H. W. Spiess, and D. Hinderberger. 2011. DEER in biological multispin-systems: a case study on the fatty acid binding to human serum albumin. *J. Magn. Reson.* 10.1016/j.jmr.2011.1003.1003.

57. Schweiger, A., and G. Jeschke. 2001. Principles of Pulse Electron Paramagnetic Resonance. Oxford University Press, Oxford, UK.

58. Cunningham, K. L., K. M. McNett, …, D. R. McMillin. 1997. EPR spectra, luminescence data, and radiationless decay processes of copper(II) porphyrins. *Inorg. Chem.* 36:608–613.